15th World Congress on Computational Mechanics (WCCM-XV)
8th Asian Pacific Congress on Computational Mechanics (APCOM-VIII)
Virtual Congress: 31 July – 5 August 2022
S. Koshizuka (Ed.)

SPHERULITE MICROSTRUCTURE FORMATION SIMULATION BASED ON EFFECT OF MOLDING CONDITIONS ON POLYLACTIC ACID

LIQIN HONG[1], KOICHI TATSUNO[2] AND YOSHITERU AOYAGI[3]

[1] Department of Finemechanics, Tohoku University
6-6-01 Aoba, Aramaki, Aoba-ku, Sendai, 980-8579, JAPAN
hong.liqin.p7@dc.tohoku.ac.jp

[2] Department of Finemechanics, Tohoku University
6-6-01 Aoba, Aramaki, Aoba-ku, Sendai, 980-8579, JAPAN
k-tatsuno@dc.tohoku.ac.jp

[3] Department of Finemechanics, Tohoku University
6-6-01 Aoba, Aramaki, Aoba-ku, Sendai, 980-8579, JAPAN
aoyagi@tohoku.ac.jp (https://web.tohoku.ac.jp/aoyagi/)

Key words: Crystalline Polymers, Polylactic Acid, Spherulite, Mechanical Properties, Monte Carlo Simulation

Abstract. *This study investigates a simulation model predicting spherulite microstructure formation based on experimental observations. The crystallization process of polylactic acid is observed at different molding temperatures by in-situ observation, and the rate of spherulite formation and growth is estimated. Furthermore, according to the Turnbull-Fisher primary nucleation model and the Lauritzen-Hoffman secondary nucleation model, Monte Carlo simulations of spherulite microstructure formation are performed based on the obtained experimental results. The validity of the method is verified by a comparison of the simulated and the experimental results.*

1 INTRODUCTION

Thermoplastic polymers are increasingly being used in a wide range of fields because of their lightweight, low cost, and excellent formability[1][2][3]. Crystalline polymers, which means thermoplastic polymers with a semicrystalline phase, have a mixture of a crystalline phase with a stable folding structure of molecular chains and an amorphous phase with a disordered structure on a microscopic scale. These two layers are alternately stacked to form a structure: lamellar crystal[4][5]. In addition, it is known that lamellar crystals grow radially to produce a microstructure, which is called a spherulite[6][7]. The mechanical properties of crystalline polymers are closely related to the dimensions of the spherulite and the crystallinity, and the morphology of spherulite depends on the molding conditions such as temperature and pressure[8][9][10].

Evaluation of the effect of the spherulite microstructure on the mechanical properties of

crystalline polymers can improve the accuracy of structural analysis. Various studies have been conducted on microstructure and crystallization models[11][12]. However, since the spherulite is a complicated structure composed of amorphous and crystalline phases, the effects of actual molding conditions on spherulite microstructure formation and changes in mechanical properties depending on spherulite microstructure remain to be clarified.

Various models have been studied to predict the microstructure from the molding conditions. For example, a prediction model called the phase-field model, which focuses on the structure formation inside spherulite crystals, has been proposed[13]. However, this phase-field model is only applicable to isothermal crystallization, not to complex temperature conditions. A cellular automaton model based on microscopic nucleation has also been proposed[14][15]. This model does not sufficiently consider the effect of temperature on nucleation. Therefore, there are still many unknowns regarding the effects of temperature, pressure, and material flow on the formation of spherulite structure during the actual forming process.

In this study, we conducted in-situ observation tests at various molding temperatures to construct a simulation method for spherulite structure formation of polylactic acid (PLA) based on experimental evaluations. First, in-situ observation tests were conducted at various molding temperatures to understand the effect of molding conditions on spherulite formation. Next, a time evolution simulation method of spherulite formation was developed, and its validity was examined. The parameters used in the numerical simulation were identified based on the obtained experimental results.

2 IN-SITU OBSERVATION TEST OF CRYSTALLIZATION PROCESS

2.1 Specimen preparation for in-situ observation tests

Figure 1 shows a schematic diagram of the specimen. PLA (IngeoRT Biopolymer 4032D, Nature Works LLC) was used as the material of the specimen. In this study, to evaluate the behavior of the spherulite structure in bulk material as much as possible, a mold made with 0.45 mm thick aluminum foil was placed on a microscope slide to prevent excessive thinning of the polylactic acid during melting and to maintain a certain thickness. Polylactic acid pellets were placed in the hole of the aluminum foil mold and heated at 200 ℃ for 60 minutes using a forced convection constant-temperature dryer (SOFW-300SB, As one Corporation). By placing a cover glass on top of the melted PLA and keeping it at 200 ℃ for further ten minutes, the specimens used for the in-situ observation test were prepared.

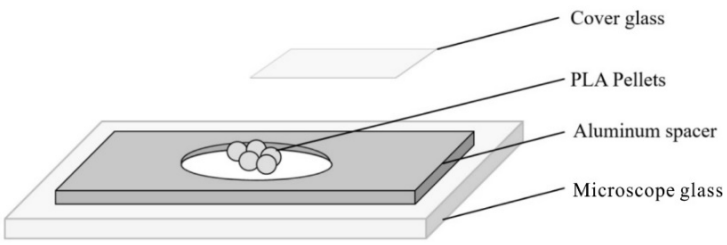

Figure 1 Details of in-situ observation test piece

2.2 In-situ observation test using polarized light microscope

A polarizing microscope (KEYENCE Digital Microscope VHX-6000) was used for an in-situ observation. The crystalline phase has an optical anisotropy so that the spherulites can be observed with the polarized light as the bright field of view. Figure 2 shows a schematic diagram of the in-situ observation of the crystallization process of polylactic acid on a heat stage. The specimens were held at 200 ℃ for 5 minutes to stabilize the temperature, then slowly cooled for ten minutes until the forming temperature, which was from 80 ℃ to 160 ℃. When it reached the forming temperature, an observation started, and photographs were taken every 15 seconds. Since it was difficult to precisely control the molding temperature in each test with the heat stage, temperatures were measured respectively for 28 specimens.

2.3 Spherulite growth rate

The spherulite growth rate is measured by observing the time evolution of the diameter of spherulites. It is assumed that there is no difference in the growth rate of each spherulite regardless of the crystallization progress in a specimen. Spherulites that had little contact with the surroundings were selected from the observed images for analysis. The average value of the change in diameter with time was obtained for the spherulite growth rate $\dot{d}$ [m/s]. Since the number of spherulites differs in each test because of the forming temperature, 3 to 15 spherulites were measured in each test.

2.4 Local nucleation rate

Figure 3 shows the schematic diagram of the spherulite number density developing with time. Note that the nucleation rate is not constant with time because the number of spherulites per unit area decreases as the amorphous area decreases. The graph of spherulite number density is approximated by

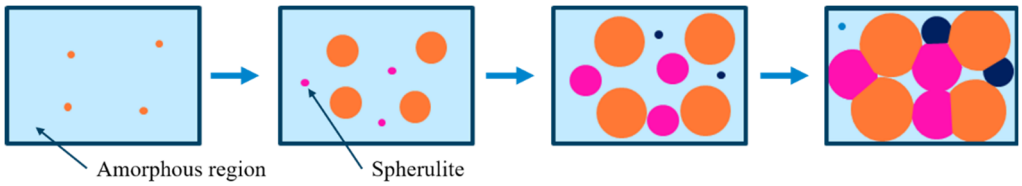

Figure 2 Change in diameter and number of spherulites

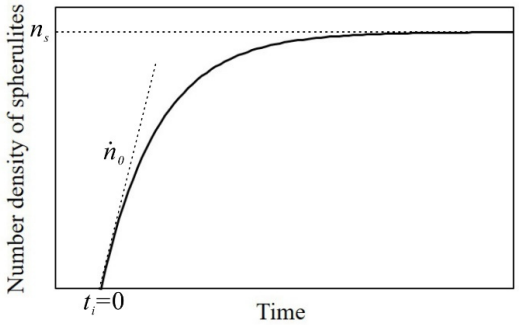

Figure 3 Change of the number density of spherulites in an observation area

$$n(t_i) = n_s \left\{ 1 - \exp\left(-\frac{\dot{n}(0)}{n_s} t_i \right) \right\} \tag{1}$$

where n_s is the spherulite number density at saturation, $\dot{n}$ is the local nucleation rate, t_i is the time when spherulite formation beginning is thought to be zero, and $\dot{n}(0)$ is the initial nucleation rate corresponding to the gradient at $t_i = 0$ in Fig. 3. The following nucleation rate was derived by differentiating Eq. (1).

$$\dot{n}(t_i) = \dot{n}(0) \exp\left(-\frac{\dot{n}(0)}{n_s} t_i \right) \tag{2}$$

The local nucleation rate at $t_i = 0$, which is independent of the number of spherulite in an observation area, corresponds to the initial nucleation rate. It is not easy and inefficient to find a moment when nucleation starts from all sequential images. Therefore, we assumed that the nucleation rate is constant for a short period of time at the early stage of spherulite generation and estimated the local nucleation rate from a single image at the early stage. The maximum diameter of the spherulite $d_{\max}$, the minimum diameter of the observable spherulite $d_{\min}$, and the number of spherulites Q whose diameter is between $d_{\max}$ and $d_{\min}$ are measured in the observation area V_t of the image at the early stage of nucleation. Set the time for the spherulite diameter reaching $d_{\max}$ from $d_{\min}$ as t_o. The difference between the maximum and minimum spherulite diameters can be expressed by

$$d_{\max} - d_{\min} = t_o \dot{d} \tag{3}$$

The relationship between the number of spherulites and the initial nucleation rate as follows

$$Q / V_t = \dot{n}(0) t_o \tag{4}$$

Therefore, by removing t_o from Eqs (3) and (4), the initial nucleation rate, i.e., the local nucleation rate, is obtained.

$$\dot{n}(0) = \frac{Q\dot{d}}{(d_{\max} - d_{\min}) V_t} \tag{5}$$

2.5 Spherulitic structure formation model

The Turnbull-Fisher model[16] and the Lauritzen-Hoffman model[17], which describe primary nucleation in the liquid phase and secondary nucleation on existing crystal surfaces, were used in this research. The primary nucleation and the secondary nucleation model are given by

$$\dot{n} = \dot{n}_0 \exp\left\{ -\frac{\Delta E_1}{RT} - \frac{K_1 T_m^{\circ 2}}{RT(T_m^{\circ} - T)^2} \right\} \tag{6}$$

$$\dot{d} = \dot{d}_0 \exp\left\{ -\frac{\Delta E_2}{RT} - \frac{K_2 T_m^{\circ}}{RT(T_m^{\circ} - T)} \right\} \tag{7}$$

The local nucleation rate $\dot{n}$ and the spherulite growth rate $\dot{d}$ obtained from the in-situ tests

were compared with the nucleation rate in the Turnbull-Fisher's primary nucleation model and the growth rate in the Lauritzen-Hoffman's secondary nucleation model, as shown in Eqs (6) and (7), respectively. The equilibrium melting temperature T_m° was set to 170 ℃ based on the physical property data of the raw PLA. K_1 is the primary nucleation factor and K_2 is the secondary nucleation factor. ΔE_1 is the energy of molecular chain transportation. ΔE_2 is the energy of molecular chain diffusion. $\dot{n}_0$ is the reference nucleation rate. $\dot{d}_0$ is the reference growth rate. Figure 4 shows a schematic diagram of the temperature dependence of spherulitic structure formation models. The primary nucleation rate reaches a peak at lower temperatures than that for secondary nucleation. This is because the critical crystal nucleus size and the Gibbs energy of the critical nucleus to the liquid are large in the temperature region where crystal growth proceeds, making nucleation practically impossible, and the critical Gibbs energy decreases to a value where primary nucleation is possible only in the temperature range with large undercooling[18]. The parameters of the spherulite formation model were identified by fitting.

2.6 Results and discussion of spherulite growth rate

In Fig. 5, the spherulite growth rate obtained by the in-situ test was compared with the secondary nucleation model. It was confirmed that the spherulite growth rate reached a peak at about 138 °C. There was some variation, but the trend was similar to that of the secondary nucleation model in the temperature range from 80 °C to 160 °C. The parameters were identified by curve fitting of the test results while setting the peak temperature to 138 ℃, as shown in

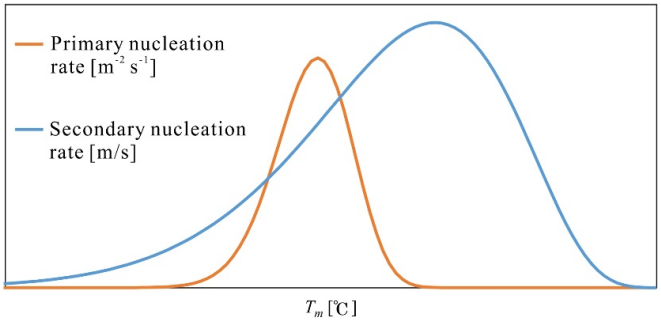

Figure 4 Temperature dependence of nucleation models

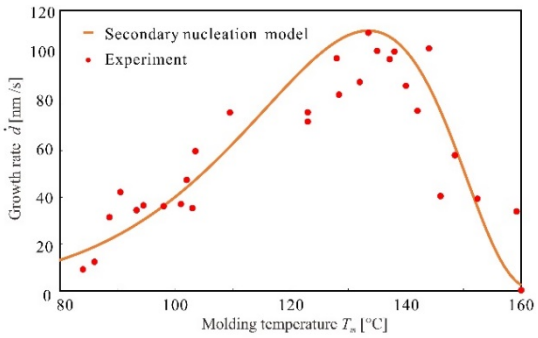

Figure 5 In-situ observation results of growth rate and identified secondary nucleation model

Table 1.

2.7 Results and discussion of local nucleation rate

Figure 6 compares the local nucleation rate determined by the in-situ test with the primary nucleation model. The results in the low-temperature range showed a larger variation than those in the high-temperature range. One of the possible reasons for this is the influence of the temperature conditions of the in-situ observation test. Because of the slow cooling, nucleation may occurs during the great range of temperature before reaching the expected value. Also, the area of the observed region may be another factor. Because the smaller spherulites diameter at lower temperature requires a magnified observation, the region actually goes smaller. Considering 103 °C as the peak, the parameters of the primary nucleation model were identified by curve fitting using the experimental results from 103 °C to 160 °C, avoiding the variation parts. The parameters are shown in Table 2. The nucleation rate's peak at 103 °C is lower than the growth rate's peak at 138 °C in Section 2.6. The position of the peak is considered to be reasonable.

Table 1 Identified parameters of rate $\dot{d}$

Growth rate $\dot{d}$ [m/s]	
$\dot{d}_0$ [m/s]	2.05×10^{3}
ΔE_2 [J]	1.21×10^{-19}
K_2 [J]	9.82×10^{-22}

Table 2 Identified parameters of rate $\dot{n}$

Nucleation rate $\dot{n}$ [m/s]	
$\dot{n}_0$ [m^{-2} s^{-1}]	1.14×10^{64}
ΔE_1 [J]	6.16×10^{-19}
K_2 [J]	1.38×10^{-21}

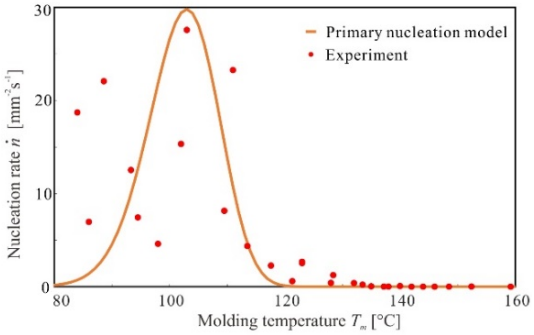

Figure 6 In-situ observation results of growth rate and identified primary nucleation model

3 DEVELOPMENT AND DISCUSSION OF A SIMULATION METHOD FOR SPHERULITE FORMATION BASED ON IN-SITU OBSERVATION RESULTS

3.1 Simulation method for spherulite formation

The Turnbull-Fisher primary nucleation model and the Lauritzen-Hoffman secondary nucleation model described in Chapter 2 were used for the simulation. The parameters were used from Tables 1 and 2.

Figure 7 shows a computational model for the simulation. A planar analysis area consisting of cells of 100 nm per side was set up. Each cell can be in either the glassy or crystalline state, and all cells are in the glassy state at the start. A random number R [0, 1] given to all cells at each computation step determines the state of the cell using

$$\begin{aligned} &R \le k_1 \\ &k_1 < R \le k_1 + k_2 \\ &k_1 + k_2 < R \end{aligned} \tag{8}$$

where k_1 is the primary nucleation probability and k_2 is the secondary nucleation probability. When $R \le k_1$, the cell transits to crystal state by the primary nucleation. When $k_1 < R \le k_1 + k_2$, the cell transits to crystal state by the second nucleation. When $k_1 + k_2 < R$, the cell stays in the amorphous phase. The probability k_1 and k_2 are determined as follows:

$$k_1 = \dot{n}_0 \exp\left\{-\frac{\Delta E_1}{RT} - \frac{K_1 T_m^{\circ 2}}{RT(T_m^{\circ} - T)^2}\right\} a^2 \Delta t \tag{9}$$

$$k_2 = \dot{d}_0 \exp\left\{-\frac{\Delta E_2}{RT} - \frac{K_2 T_m^{\circ}}{RT(T_m^{\circ} - T)}\right\} m\Delta t \Big/ a \tag{10}$$

Here a is the side length of a cell, 1×10^{-7} m. Δt is the step of computation, 0.1s. m is the number of adjacent crystal points in the four neighborhoods around the target cell, ranging from 1 to 4.

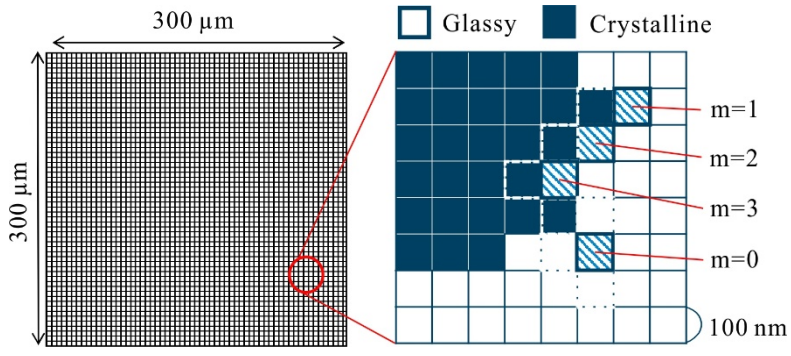

Figure 7 Monte Carlo method is used to simulate the spherulite formation and growth in a 300 μm square area. The crystalline phase is randomly generated, and the probability is influenced by the situation in the neighbor region.

3.2 Discussion of the effect of the slow cooling stage on the local nucleation rate

Here the simulation method developed in section 3.1 is used to evaluate the numerical model described in section 2.7. The analysis area is 300 μm square. Forming temperatures were analyzed in 1 °C increments in the range from 80 °C to 120 °C. Figure 8(a) shows the simulated local nucleation rate and the primary nucleation rate calculated using Eq. (6). Figure 8(b) shows the simulated image of local nucleation of two minutes after reaching the expected molding temperature of 117 °C. The microcells that transitioned to the crystalline state by the primary nucleation were represented by different colors, while the cells that transitioned by the secondary nucleation were the same color as the adjacent crystalline state cells.

In Fig. 9, the local nucleation rate in the simulation results, including the slow cooling step, follows the primary nucleation model, which corresponds to the experimental results, in the range of molding temperatures from 110 °C to 120 °C. However, the simulation results from 90 °C to 110 °C was much lower than that of the model. This may be due to the fact that $d_{\max}$ is larger than expected because the formation starts earlier than expected, as described in section 2.7. In fact, in the in-situ observation at 98 °C, it can be confirmed that spherulites had already formed before the temperature reached 98 °C.

It was considered that spherulite was affected in the temperature range below 103 °C, which was considered the peak. However, there was also a possibility that the influence occurs even

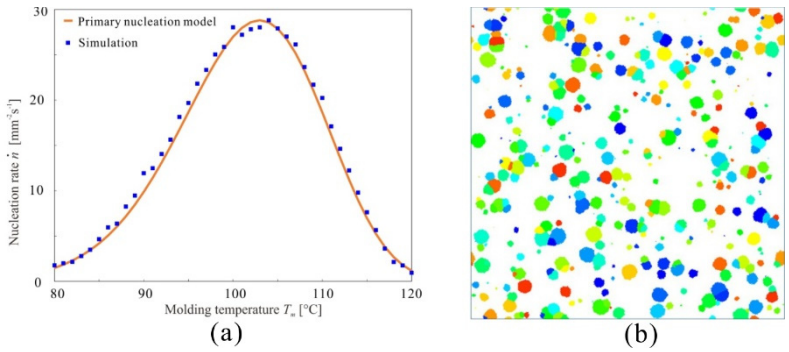

Figure 8 (a) Comparison between nucleation rate from simulation results and identified primary nucleation model and (b) simulation image for 300 μm square

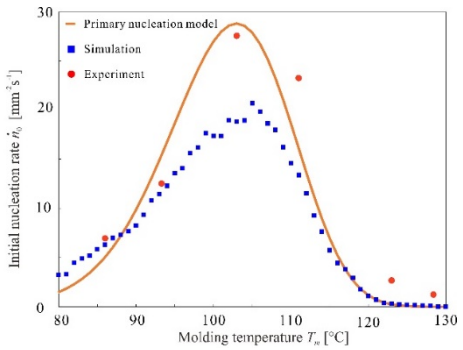

Figure 9 Comparison between nucleation rate from simulation with cooling process and typical in-situ observation results, and identified primary nucleation model

around 110 °C. In the range from 80 °C to 90 °C, the simulation results were slightly higher than the model. Considering that the cooling time was set to 10 minutes regardless of the molding temperature, the cooling rate is higher in the range from 80 °C to 90 °C. Since the local nucleation rate is considered to be low at these temperatures, the $d_{\max}$ from 80 °C to 90 °C was strongly affected by the increasing number of generation of spherulites, rather than the measurement of $d_{\max}$ as a larger value than expected. Therefore, it was confirmed that the local nucleation rate is significantly affected by the slow cooling process.In Fig. 9, the in-situ observation results at 86, 93, 113, 123, and 128 °C are also shown. Since the primary nucleation model was fitted from the in-situ test results, they are certainly close. However, the simulation results tended to differ significantly from observation results. In order to get the local nucleation rate of simulation considering the slow cooling process close to the value of the in-situ observation results, the parameters of the primary nucleation model should be re-identified.

Table 3 shows the new parameters. Since there is a large variation at temperatures below 103 °C, the parameters of the primary nucleation model were re-identified by preferentially fitting the results above 103 °C. Figure 10 shows some in-situ observation results which are close to simulation results and the curve given by the primary nucleation model with the re-identified parameters. The re-identified curve tends to be higher than the in-situ observation results. The observation just measured the apparent nucleation rate. We find that the actual local nucleation rate is larger than that measured by the observation.

3.3 Comparison of in-situ observation results and spherulite formation simulations

Figure 11 shows the simulated microstructures and the in-situ observation results at the

Table 3 Re-identified parameters of rate $\dot{n}$

Nucleation rate $\dot{n}$ [m/s]	
N_0 [m^{-2} s^{-1}]	5.29×10^{35}
ΔE_1 [J]	3.05×10^{-19}
K_2 [J]	6.82×10^{-22}

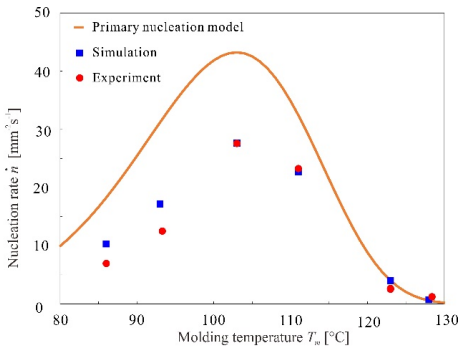

Figure 10 Comparison between nucleation rate from simulation with cooling process and typical in-situ observation results, and re-identified primary nucleation model

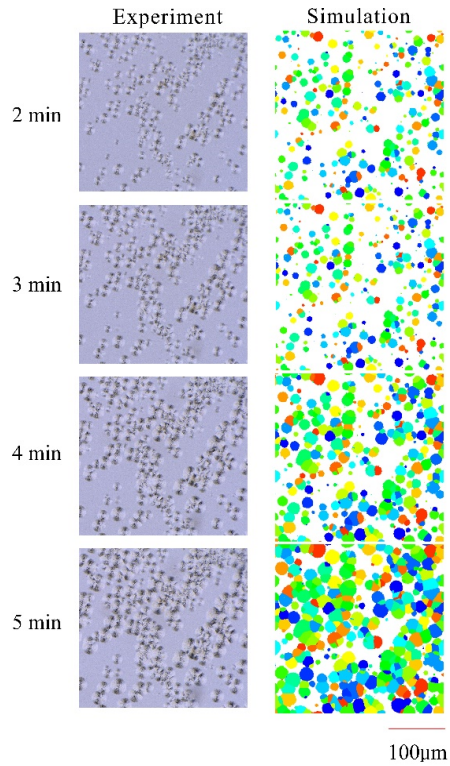

Figure 11 In-situ observations and simulation results at 117 °C

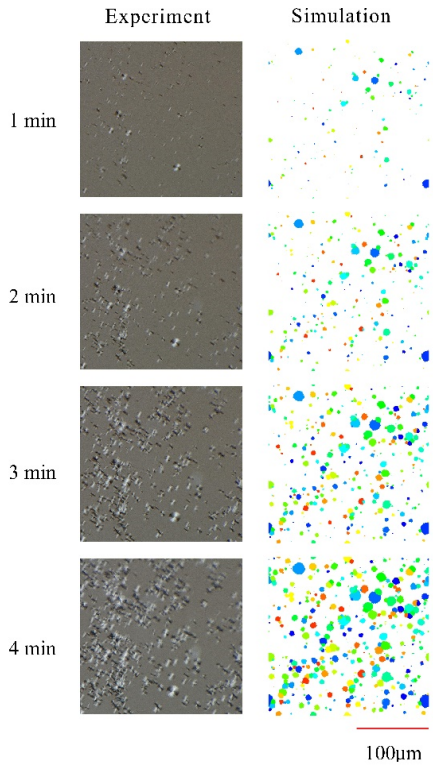

Figure 12 In-situ observations and simulation results at 93 °C

molding temperature of 117 °C, also the time after reaching the expected molding temperature. In Fig. 11, the primary nuclei generated in the glassy region grow spherically and collide with each other to form spherulite boundaries, reproducing the characteristic spherulite structure. The simulation results cannot be directly compared with the in-situ observation test results regarding the number of spherulite crystals because some are too small to be observed in the in-situ observation test results. However, the simulation results show similar trends in the size of spherulites and the percentage of glassy regions at each time to the in-situ observation test results, which is considered to be a good representation of spherulite formation over time. Figure 12 shows the comparison at 93 °C. Similar to Fig. 11, the size of the spherulites and the percentage of glassy regions show similar trends to the in-situ observation test results, confirming the simulation method's validity.

4 CONCLUSION

The primary and secondary nucleation rates were calculated based on the in-situ observation tests. A simulation method for spherulite structure formation was developed, representing the local nucleation rate and spherulite growth rate in a planar region. The conclusions are summarized as follows.

(1) The local nucleation rates obtained from the in-situ tests scatter widely in the range of forming temperatures 80 - 103 °C, making it difficult to represent them with a primary nucleation model.

(2) The spherulite formation simulation results show that the slow cooling stage affects the local nucleation rate significantly.
(3) The simulation method, which considered the slow cooling stage, could represent spherulite formation numerically.

ACKNOWLEDGMENTS

This work was performed with the support of JSPS KAKENHI Grant Number 21K03745.

REFERENCES

[1] Ning, H., Vaidya, U., Janowski, G. M. and Husman, G., *Design manufacture and analysis of a thermoplastic composites frame structure for mass transit.* Composite Structures, Vol. 80, No. 1 (2007), pp. 105–116.
[2] Pimenta, S. and Pinho, S. T., *Recycling carbon fibre reinforced polymers for structural applications*. Waste Management, Vol. 31, No. 2 (2011), pp. 378–392.
[3] Chen, Q., Boisse, P., Park, C. H., Saouab, A. and Breard, J., *Intra/inter-ply shear behaviors of continuous fiber reinforced thermoplastic composites in thermoforming processes.* Composite Structure, Vol. 93, No. 7 (2011), pp. 1692–1703.
[4] Wlochowicz, A. and Eder, M., *Distribution of lamella thicknesses in isothermally crystallinzed polypropylene and polyethylene by differential scanning calorimetry.* Polymer, Vol. 25, No. 9 (1984), pp. 1268–1270.
[5] Spieckermann, F., Wilhelm, H., Kerber, M., Schafler, E., Polt, G., Bernstoff, S., Ad-diego, F. and Zehetbauer, M., *Determination of lamella thickness distributions in isotactic polypropylene by x-ray line profile analysis.* Polymer, Vol. 51, No. 18 (2010), pp. 4195–4199.
[6] Zheng, Q., Shangguan, Y., Yan, S., Song, Y., Peng, M. and Zhang, Q., *Structure, morphology and non-isothermal crystallization behavior of polypropylene catalloys.* Polymer, Vol. 46, No. 9 (2005), pp. 3163–3174.
[7] Zhou, J. J., Liu, J. G., Yan, S. K., Dong, J. Y., Li, L., M., Chan C. and Schultz, J. M., *Atomic force microscopy study of the lamellar growth of isotactic polypropylene.* Polymer, Vol. 46, No. 12 (2005), pp. 4077–4087
[8] Fujiyama, M. and Azuma, K., *Skin/core morphology and tensile impact strength of injection-molded polypropylene.* Journal of Applied Polymer Sciense, Vol. 23, No. 9 (1979), pp. 2807–2811.
[9] Wright, Dunk R. Bouvart D., D. G. M. and Autran, M., *The effect of crystallinity on the properties of injection moulded polypropylene and polyacetal.* Polymer, Vol. 29, No. 5 (1988), pp. 793–796.
[10] Schrauwen, Breemen L. C. A. v. Spoelstra A. B. Govaert L. E. Peters G. W. M., B. A. G. and Meijer, H. E. H., *Sturucture, deformation, and failure of flow-oriented semicrystalline polymers.* Macromolecules, Vol. 37, No. 23 (2004), pp. 8618–8633.
[11] Avrami, M., *Granulation, phase change, and microstructure kinetics of phase change. iii.* The Journal of Chemical Physics, Vol. 9, No. 2 (1941), p. 177.
[12] Cao, J., Kikutani, T., Takaku, A. and Shimizu, J., *Nonisothermal orientation‐induced crystallization in melt spinning of polypropylene.* Journal of Applied Polymer Science, Vol. 37, No. 9 (1989), pp. 2683–2697.

[13] Granasy, L., Pusztai, T., Tegze, J., Warren, J. A. and Douglas, J. F., *Growth and form of spherulites*. Physical Review, Vol. E72, No. 1 (2005), p. 011605.
[14] Raabe, D., *Mesoscale simulation of spherulite growth during polymer crystallization by use of a cellular automaton.* Acta Materialia, Vol. 52, No. 9 (2004), pp. 2653–2664.
[15] Raabe, D. and Godara, A., *Mesoscale simulation of the kinetics and topology of spherulite growth during crystallization of isotactic polypropylene (ipp) by using a cellular automaton.* Modelling and Simulation in Materials Science and Engineering, Vol. 13, No. 5 (2005), pp. 733–751.
[16] Turnbull, D. and Fisher, J. C., *Rate of nucleation in condensed systems*. Journal of Chemical Physics, Vol. 17 (1949), pp. 71–73.
[17] Lauritzen, J. I. and Hoffman, J. D., *Crystallization of bulk polymers with chain folding: Theory of growth of lamellar spherulites.* Journal of Research of the National Bureau of Standards, Vol. 65A (1961), pp. 297–336.
[18] T.Hikima, M.Oguni, M.Hanaya, *Low-temperature crystallization in fragile liquids.* Netsu Sokutei, Vol. 26, No. 5 (1999), pp. 173–185.